Regioregularity effects in the chain orientation and optical anisotropy of composite polymer/fullerene films for high-efficiency, large-area organic solar cells

Shang-Yu Chuang, Hsuen-Li Chen,* Wen-Hao Lee, Yu-Ching Huang, Wei-Fang Su, Wei-Ming Jen and Chun-Wei Chen

Received 10th March 2009, Accepted 15th May 2009
First published as an Advance Article on the web 10th July 2009
DOI: 10.1039/b904870g

In this paper, we demonstrate the strong influence of the regioregularity (RR) of poly-(3-hexylthiophene) (P3HT) on the optical anisotropy of hybrid P3HT/fullerene films before and after thermal annealing. We determined the conversion efficiency and characterized the optical anisotropy of P3HT/6,6-phenyl-C61-butyric acid methyl ester (PCBM) blends featuring various values of RR. Unlike grazing-incidence X-ray diffraction analysis, optical anisotropic measurement provides a clear and convenient view of the polymer orientation and the device anisotropic absorption at the same time. By calculating the in-plane and out-of-plane optical constants (extinction coefficients and refractive indices), we determined that the optical anisotropy of P3HT/PCBM films was improved in both orientations upon increasing the RR. Upon increasing the thermal annealing temperature, the main chains of high-RR P3HT were converted from an amorphous structure to an alignment parallel to the substrate, resulting in higher optical anisotropy. The degree of anisotropy of the high-RR P3HT/PCBM blend was up to six times higher than that of the low-RR sample. This strong RR effect on optical anisotropy was also evident in the power conversion efficiency of large-area P3HT/PCBM-based organic solar cells.

Introduction

Because of its solution processability, low cost, and compatibility with flexible substrates, organic solar cells based on poly(3-hexylthiophene) (P3HT)/6,6-phenyl-C61-butyric acid methyl ester (PCBM) hybrid films and bulk heterojunction (BHJ) structures have attracted much attention recently.[1–6] Reasonable power conversion efficiencies (PCEs) have been achieved, with efficient light-induced charge separation due to the large-area donor–acceptor interface of the BHJ.[7–13] The self-organizing properties of pristine P3HT lead to the high quality of its crystalline and aligned orientations. The morphology of a polymer thin film has a significant influence on its optoelectronic and device performance. [6] To increase the quality of the donor–acceptor interface, PCBM is often introduced into hybrid systems, even though its nanostructure interferes with the self-organizing ability of P3HT.[14,15] Many crystallization treatment processes, such as thermal annealing[3,16–18] and solvent annealing,[19–21] can be applied to recover the extended and aligned morphology in P3HT films. Because PCBM diffuses and aggregates under thermal processing, P3HT can convert into crystallites in PCBM-free regions.[4–6,22] For the analysis of polymer crystallites, the orientation of the polymer chains can be determined using grazing-incidence X-ray diffraction (GIXRD).[4,5,23–25]

The anisotropic properties of polymer thin films, based on the preferential orientation of the polymer main chains, strongly influence their optoelectronic properties, including their carrier mobilities and optical absorptions. Previous studies have demonstrated the effects of several kinds of polymer anisotropic properties.[26–31] Optical anisotropy is determined from measurements of the polarized reflection and transmission spectra of anisotropic films. The degree of anisotropy is measured in terms of the preferential chain conformation parallel or perpendicular to the substrate. The electric field of incident light aligned parallel to the direction of the polymer main chains, *i.e.*, the orientation of the transition dipole moments, results in π–π^* absorption. Although the anisotropy of conjugated polymers has been studied thoroughly, very little research has focused on the relationship between the BHJ and the optical anisotropic properties of hybrid films.[32] BHJ cells incorporating P3HT/PCBM blends are more efficient than other types of structures, such as single- or bi-layer organic solar cells. Studying the optical anisotropy of BHJs is a convenient method of determining the orientation of the polymer main chain in the PCBM domain. Although thermal annealing is a critical factor that affects the orientation of polymer main chains,[22,33,34] the relationships between the P3HT/PCBM optical anisotropy, the polymer backbone orientation, and the degree of regioregularity (RR) during the annealing process for large-area solar cells have not been reported previously.

The anisotropy of polymeric materials is related to their crystallinity, which correlates to the orientation and the inter-chain packing of the polymer chains.[26,27] In such oriented morphologies, the optical properties become anisotropic when there is a high degree of main chain alignment and extension. There are three possible crystalline orientations of P3HT/PCBM

Department of Materials Science and Engineering, National Taiwan University, Taipei, Taiwan. E-mail: hsuenlichen@ntu.edu.tw; Fax: +886-2-23634562; Tel: +886-2-33663240

systems.[23,24] The most preferable orientation of the polymer backbones is parallel to the thin film's surface, resulting in improved in-plane electron mobility and poor out-of-plane mobility. Because the electric field of the incident light is aligned parallel to this preferable backbone orientation, the absorption of light is significant. Therefore, distinct absorptions result from polymers aligned orthogonally perpendicular (TE) and parallel (TM) to the plane of the incident light. By measuring the reflectance and transmittance spectra of polarized light, the optical anisotropic properties of P3HT/PCBM blends can be obtained. The degree of optical anisotropy depends on the angular distribution of the polymer chains. For a system exhibiting higher optical anisotropy, the main chains oriented parallel to the substrate are more aligned. To determine the optical anisotropy of hybrid P3HT/PCBM films, optical constants are acquired using ellipsometry and optical spectrometry. The incident light for anisotropic analysis can be separated into two orthogonal electric field components, *i.e.*, perpendicular and parallel to the substrate.

The degree of RR is defined as the fraction of monomers adopting a head-to-tail configuration, rather than a head-to-head arrangement. A higher RR results in closer packing of the P3HT stacking planes, which plays an important role in determining the orientation of the polymer chains. A previous study revealed that the performance of a solar cell can be improved through the enhanced optical absorption and transport resulting from the organization of P3HT chains and domains;[14,15] the relationships between the polymer's RR, the annealing conditions, and the optical anisotropy of the BHJ have, however, not been reported previously. We have found that optical anisotropy is a useful and convenient method for determining the orientation of polymer main chains possessing various RRs.

In this paper, we focus on the influence of the RR on the optical anisotropic properties of polymer films prepared under various annealing conditions. During thermal annealing, both 90.2% and 96.7% RR P3HT samples undergo crystallization. The P3HT morphology of the low-RR sample was converted mainly into in-plane ($\parallel$) and out-of-plane ($\perp$) orientations, whereas the high-RR sample's main chains were mostly oriented in-plane ($\parallel$). To characterize the extent of ordering upon thermal annealing, we used confocal laser scan microscopy (CLSM) of P3HT/PCBM thin films to determine the distribution of PCBM. Furthermore, we present the influence of the RR on the optical anisotropy, including the ratio of the in-plane ($\parallel$) and out-of-plane ($\perp$) extinction coefficients, to demonstrate that high-RR P3HT prefers to orient itself in a specific direction during crystallization.

Experimental

In the experimental part, BK7 glass substrates were cleaned with acetone and isopropanol in an ultrasonic bath, rinsed with deionized water, and then dried with nitrogen gas. For optical measurements, P3HT/PCBM films were spun on glass substrates. P3HT polymers having RRs of 90.2 and 96.7% were synthesized using the Merck synthetic method and end-capped with hydrogen. The BHJ polymer was prepared from a solution of P3HT and PCBM (1:0.8 w/w) in chlorobenzene (CB). The thickness of the P3HT/PCBM films was characterized using an ellipsometer. The P3HT/PCBM films were spun at 800 rpm for 60 s and then they were thermally annealed at various temperatures, ranging from room temperature to 120 °C. The optical constants—namely, the refractive index (n) and the extinction coefficient (k)—of P3HT/PCBM films featuring various RR values and prepared under various annealing conditions were determined from ellipsometric and reflectance–transmittance measurements.[11–16] Ellipsometric parameters ($\tan\Psi$ and $\cos\Delta$) determined at wavelengths ranging from 350 to 850 nm were acquired using a SOPRA ellipsometer. Transmittance and reflectance spectra of the P3HT/PCBM films were recorded using a Hitachi U-4100 optical spectrometer. The measured data were fit to a dispersion function, also called an oscillator model describing the dielectric function. Oscillator models require only a few oscillator coefficients to describe both real and imaginary parts of the refractive index accurately over a very wide spectral range. Confocal laser scanning microscopy (CLSM) images were collected using a WITec CMR 200 Scanning Near-field optical microscope (SNOM) operated in the confocal mode.

The X-ray diffraction (XRD) spectra of P3HT/PCBM hybrid films before and after thermal annealing were measured using grazing-incidence X-ray-diffraction (GIXRD) in synchrotron X-rays (out-of-plane scanning mode). For measurement of their photovoltaic device performance, solar cells were fabricated under ambient conditions. Indium tin oxide-coated (ITO) glass substrates were etched with acid and then cleaned with chloroform, acetone, and deionized water in an ultrasonication bath. The cleaned ITO samples were immediately spin-coated at 1500 rpm with a 30 nm thick layer of poly(3,4-ethylenedioxythiophene) : poly(styrene sulfonate) (PEDOT:PSS). The PEDOT:PSS-coated samples were then heated at 110 °C for 5 min. The active layer of P3HT:PCBM (1:0.8; RR = 90.2 or 96.7%) was then spin-coated to form a thin film having a thickness of 80–95 nm. The samples were then placed in a vacuum chamber, where an aluminium electrode (100 nm) was deposited through a mask, leaving an active area ranging from 4 to 400 mm^2; these samples were then annealed at 120 °C for 15 min. The photovoltaic device efficiency was measured under simulated AM1.5 illumination conditions.

Results and discussion

As a self-organizing polymer, the nanostructure of P3HT depends strongly on its degree of RR. Because more of its monomer units adopt a head-to-tail configuration, higher-RR P3HT is able to pack with closer stacking of its planes. In a BHJ photovoltaic device, the fullerene derivative PCBM is introduced, which disturbs the distribution of the P3HT crystalline domains in various ways, including the packing within the domains and the relative domain orientations. Therefore, it is assumed that the presence of P3HT crystallites at high or low RR is limited to a fair degree by the presence of PCBM in the absence of thermal annealing. Unraveling the complex morphology of P3HT/PCBM hybrid systems remains a significant challenge. One potentially useful strategy is measuring the anisotropy of the optical constants n and k: a higher refractive index indicates a denser structure and an enhanced extinction coefficient for the absorption band is caused by crystallization of the polymer material. To obtain the optical constants of P3HT/PCBM blends

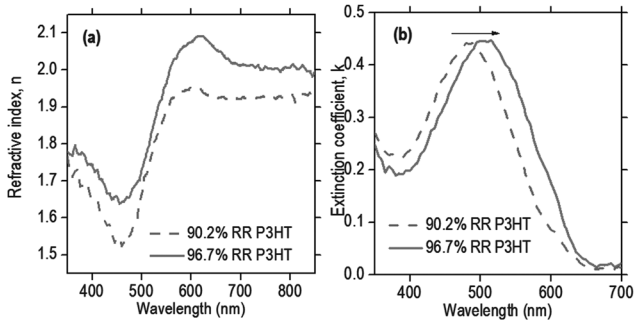

Fig. 1 (a) Refractive indices and (b) extinction coefficients of 90.2% and 96.7% RR P3HT in P3HT/PCBM hybrid films.

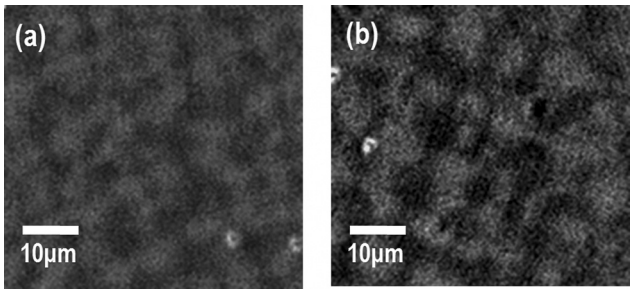

Fig. 3 Confocal laser scan microscopy images of P3HT/PCBM blends annealed for (a) 0 and (b) 10 min.

featuring distinct RRs, we recorded their reflectance and transmittance spectra and performed ellipsometry measurements ($\tan\Psi$, $\cos\Delta$). Fig.1 (a) and (b) display the refractive indices and extinction coefficients of P3HT/PCBM, respectively, for the two vales of RR. For an absorption band, the refractive index will be lower for an abnormal dispersion. The higher refractive index of the 96.7% RR P3HT illustrates that the RR influences chain stacking, resulting in denser packing within a coil conformation. Because more of its monomer units adopt a head-to-tail configuration, the higher RR of this polymer enables closer packing of its main chains. The value of the extinction coefficient corresponds to the degree of crystallization, which is due to the ordered alignment of polymer main chains absorbing light strongly *via* π–π^* transitions. Prior to performing the annealing process, the extinction coefficients of the absorption peaks of the P3HT/PCBM blends were both *ca.* 0.4. The introduction of PCBM was the main cause of the disruption of the P3HT crystallinity, leading to the low absorption of light in both the high- and low-RR samples. The red-shift in the absorption of the 96.6% RR P3HT sample was due to greater stacking of its polymer backbones.[10]

Next, we investigated the influence of thermal annealing upon the P3HT/PCBM hybrid structures. Because the main absorption peaks of the 90.2% and 96.7% RR P3HT polymers appear at 490 and 510, respectively, we compared the optical constants of each absorption to determine the effects of thermal annealing at various temperatures. Fig. 2 reveals that the refractive index and extinction coefficient of the high-RR P3HT increased significantly upon increasing the thermal annealing temperature from

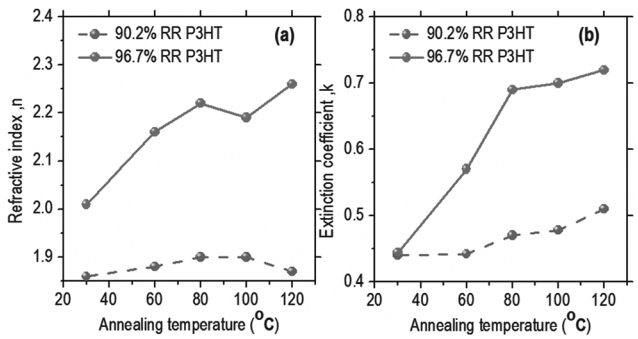

Fig. 2 (a) Refractive indices and (b) extinction coefficients of 90.2% and 96.7% RR P3HT in P3HT/PCBM blends that had been annealed at various temperatures.

room temperature to 120 °C; in contrast, we observed no striking changes for the low-RR polymer. In this discussion, we focus on the variation in the extinction coefficient, which is related to the extent of crystallization. The amount of π–π^* absorption, derived from value of k, was nearly the same for both the non-annealed 96.7% and 90.2% RR P3HT polymers. As a result of its distinct ability to pack with a higher degree of crystallinity, the extinction coefficients of the 96.7% and 90.2% RR P3HT/PCBM blends annealed at 120 °C were enhanced by 1.62 and 1.15 times, respectively, relative to those of their non-annealed samples. Thermal treatment leads to PCBM aggregation, providing PCBM-free regions for P3HT extension and crystallization (Fig. 3). After this change in morphology, the high-RR P3HT exhibited pronounced inter-plane stacking, which led to a significant enhancement of the optical absorption of its aligned crystalline domain. In the case of the low-RR polymer, the degree of extension and alignment of the P3HT main chains was restricted by the presence of more head-to-head monomer configurations.

To verify the crystallinity of P3HT/PCBM hybrid films with ordered aggregates, the X-ray diffraction spectra (incident angle $\theta_{IN} = 0.5°$, wavelength = 1.027 nm) were used to carry out the crystallinity measurement. Fig. 4(a) displays the X-ray diffraction profiles of 90.2% RR P3HT/PCBM hybrid films with respect to the different annealing temperature. The main diffraction angle $2\theta = 5.4°$ could be obtained in all the P3HT/PCBM hybrid films, which is assigned to the diffraction of the crystallographic (100) plane of P3HT.[4,5] Upon increasing the annealing temperature, the diffraction intensities are significantly increased. It gives direct evidence that annealing process is attributed to the conversion of P3HT/PCBM hybrid films from an amorphous structure to a crystalline one. Fig. 4(b) displays the X-ray diffraction profiles measured from the 96.7 RR P3HT/PCBM hybrid films under the same annealing process. The RR effect of P3HT is clearly observed in the relatively higher diffraction intensities than for 90.2% RR P3HT/PCBM films.

To characterize the influence of the thermal annealing process on the morphology of the various RR P3HT polymers, we measured the optical anisotropy. The model we used to determine the optical constants of P3HT/PCBM blends was adjusted to distinguish only between light propagating in-plane ($\parallel$) and out-of-plane ($\perp$)—namely, the uniaxial model. Ellipsometry measurements and polarized reflectance and transmittance spectra at various incidence angles are required to model the measured data in the uniaxial system. In the curve fitting process,

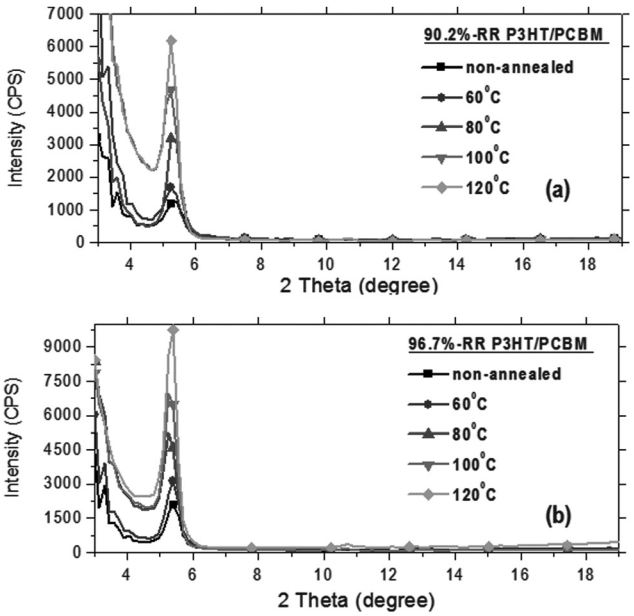

Fig. 4 X-Ray diffraction spectra of P3HT/PCBM hybrid films before and after annealing with different annealing temperature: (a) obtained from 90.2% RR P3HT/PCBM; (b) obtained from 96.7% RR P3HT/PCBM.

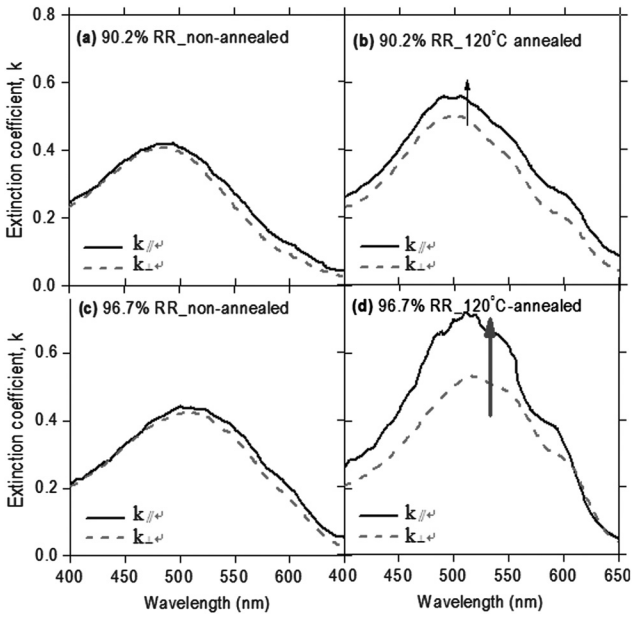

Fig. 5 In-plane and out-of-plane extinction coefficients of (a) non-annealed 90.2% RR P3HT/PCBM films; (b) 90.2% RR P3HT/PCBM films annealed at 120 °C; (c) non-annealed 96.7% RR P3HT/PCBM films, (d) 96.7% RR P3HT/PCBM films annealed at 120 °C.

the TE polarized curve was fitted to acquire the in-plane (∥) optical constants; the TM polarized curve was then fitted to obtain the out-of-plane (⊥) optical constants. This process was continued until we acquired self-consistent values, with which the theoretical data from the birefringence optical model corresponded to the measured data. We found that the optical absorption of the hybrid thin films depended on the electric field direction of the incident light. The absorption was stronger when the electric field of the incident light was aligned parallel to the orientation of the polymer transition dipole moment, *i.e.*, the direction of main chains, rather than when it was perpendicular. To determine the orientations of the P3HT backbones, we focus here on the extinction coefficients in the dispersion spectra of various samples. The peak values of $k_{\perp}$ and $k_{\parallel}$ were nearly the same, indicating that the intrinsic anisotropy of the non-annealed P3HT/PCBM blend was hindered by the random coil morphology of the main chains. Fig. 5 (a) and (b) reveal that annealing the low-RR P3HT/PCBM blend at 120 °C has an effect on the optical anisotropy, with values of $k_{\parallel}$ and $k_{\perp}$ of 0.55 and 0.48, respectively. Therefore, the observed optical anisotropy indicates that a distinct number of P3HT backbones were extended and aligned in the in-plane (∥) and out-of-plane (⊥) directions. More polymer chains lie in the plane of the film after thermal annealing. We attribute these results to the preferential orientation of P3HT crystallites in the PCBM-free regions when PCBM aggregation was occurring under thermal annealing.

For comparison, we characterized the effects of thermal annealing on the structural conversion of the high-RR P3HT/PCBM hybrid. Fig. 5 (c) and (d) display the extinction coefficients of the 96.7% RR P3HT/PCBM blend before and after thermal treatment, respectively. The values of $k_{\parallel}$ and $k_{\perp}$ of 0.72 and 0.52, respectively, for the sample annealed at 120 °C indicate an anisotropic chain conformation, confirming that thermal treatment had an affect on the P3HT/PCBM hybrid films. The larger difference in anisotropy of the annealed 96.7% RR P3HT/PCBM blend, relative to that of the low-RR sample, reveals that the RR has a dramatic effect on the degree of polymer anisotropy.

The degree of anisotropy can be defined simply as the ratio between the π–π* absorptions parallel and perpendicular to a substrate, which is related to the value of $k_{\parallel}/k_{\perp}$. If the polymer main chains are uniformly distributed, it would follow that the value of $k_{\parallel}/k_{\perp}$ would be 1. Fig. 6 displays the degrees of anisotropy of the 90.2% and 96.7% RR P3HT polymers with respect to the annealing temperature. Because of P3HT crystallization and the polymer main chains' preferential orientation, the anisotropy of P3HT/PCBM increased upon increasing the annealing temperature. The significant anisotropy we measured for the 96.7% RR P3HT/PCBM blend after thermal annealing provided much larger values of $k_{\parallel}/k_{\perp}$ than those for the random coil conformation of the polymer, implying that the crystallization domains were oriented primarily in-plane (∥). The degrees of anisotropy for the 90.2% and 96.7% RR P3HT/PCBM blends annealed at 120 °C, represented by distinct values of $k_{\parallel}/k_{\perp}$ of 1.09 and 1.59, respectively, reveal, however, the more

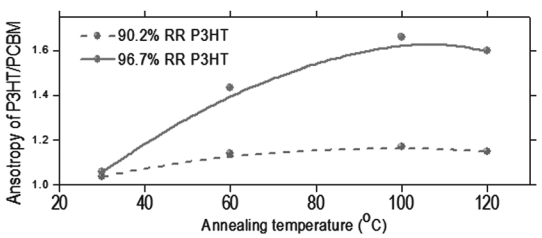

Fig. 6 Anisotropy ($k_{\parallel}/k_{\perp}$) of 90.2% and 96.7% RR P3HT/PCBM blends plotted with respect to the annealing temperature.

pronounced anisotropic nature of the high-RR sample. From the significant degree of anisotropy, the RR effect is clearly observed: the higher the RR of the P3HT polymer, the stronger its ability to pack chains in an aligned manner, indicating that the preferential in-plane (∥) oriented crystalline domains are most pronounced. Therefore, during the morphological conversion of the P3HT/PCBM blends, the high-RR P3HT backbones crystallize mainly from random coil conformations to crystalline domains that are aligned with the plane of the substrate.

We have investigated the distribution of polymer main chains by observing the extinction coefficients and using the uniaxial model. In this study, $k_{\parallel}$ and $k_{\perp}$ represent the contents of polymers aligned parallel and perpendicular to the substrate, respectively. Because the self-organizing ability of P3HT is hindered by the presence of PCBM, we found that the typical random coil conformation of the polymer main chains, *i.e.*, the amorphous morphology, was present in P3HT/PCBM BHJ structures. Therefore, we obtained near-equal values of $k_{\parallel}$ and $k_{\perp}$ for the non-annealed P3HT/PCBM samples. The slightly higher values of $k_{\parallel}$ that we obtained were not too surprising because the preferred chain orientation of the conjugated polymer is in-plane (∥). During thermal annealing, three possible morphological conversions occur for the P3HT/PCBM hybrid structure from an optical perspective:

(i) $k_{\parallel}$ increases and $k_{\perp}$ decreases, indicating that the perpendicular part of the amorphous polymer converts to a parallel crystallinity;

(ii) $k_{\parallel}$ decreases as $k_{\perp}$ increases, indicating that the parallel part of the amorphous polymer converts to perpendicular crystallinity; and

(iii) both $k_{\parallel}$ and $k_{\perp}$ increase, indicating that the amorphous polymer converts to both parallel and perpendicular crystallinity domains.

Fig. 7 (a) and (b) display the in-plane (∥) and out-of-plane (⊥) extinction coefficients of the 90.2% RR P3HT/PCBM blends subjected to various annealing temperatures. Upon increasing the annealing temperature, the value of $k_{\parallel}$ increased from 0.44 to 0.72 and that of $k_{\perp}$ increased from 0.39 to 0.48. Because both the in-plane (∥) and out-of-plane (⊥) extinction coefficients were enhanced, the morphological conversion presumably occurred through mechanism (iii), i.e., the random coil conformation of the low-RR P3HT was transformed into both in-plane (∥) and out-of-plane (⊥) crystallinity orientations. Moreover, the more pronounced change in $k_{\parallel}$ suggests that the preferential orientation of the crystallinity lies mainly parallel to the substrate. We obtained similar results from a study of high-RR P3HT/PCBM hybrid films subjected to various annealing temperatures [Fig. 7 (c) and (d)]. Fig. 8 (a) presents an illustration of the morphologies of the high- and low-RR P3HT/PCBM samples during the annealing process. The introduction of PCBM into the hybrid system interfered with the self-organization of P3HT, resulting in an amorphous distribution of P3HT/PCBM. After thermal annealing, PCBM diffused into larger clusters, allowing P3HT to convert into crystallites in PCBM-free regions. Fig. 8 (b) displays the variations in the values of $k_{\parallel}$ and $k_{\perp}$ for the 90.2% and 96.7% RR P3HT/PCBM samples upon varying the annealing temperature. The orientation of P3HT is clearly described by these values. In the structural conversion of the hybrid, both $k_{\parallel}$ and $k_{\perp}$ increased upon increasing the annealing temperature, indicating

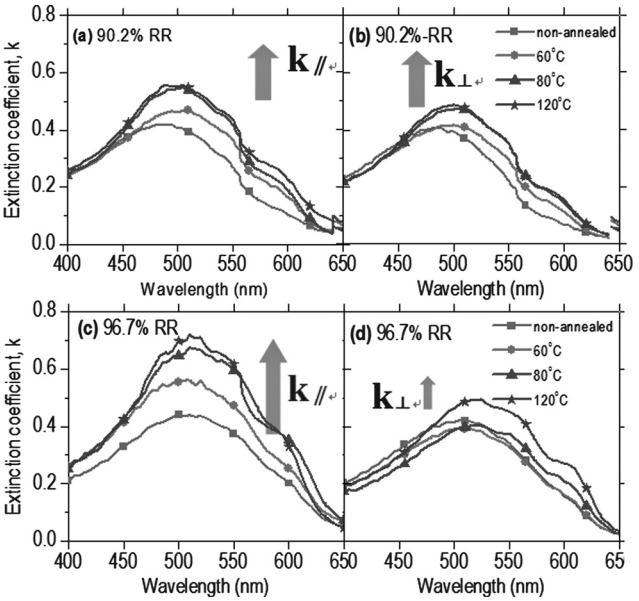

Fig. 7 Extinction coefficients of the (a) in-plane and (b) out-of-plane components of 90.2% RR P3HT/PCBM and of the (c) in-plane and (d) out-of-plane components of 96.7% RR P3HT/PCBM, plotted with respect to the annealing temperature.

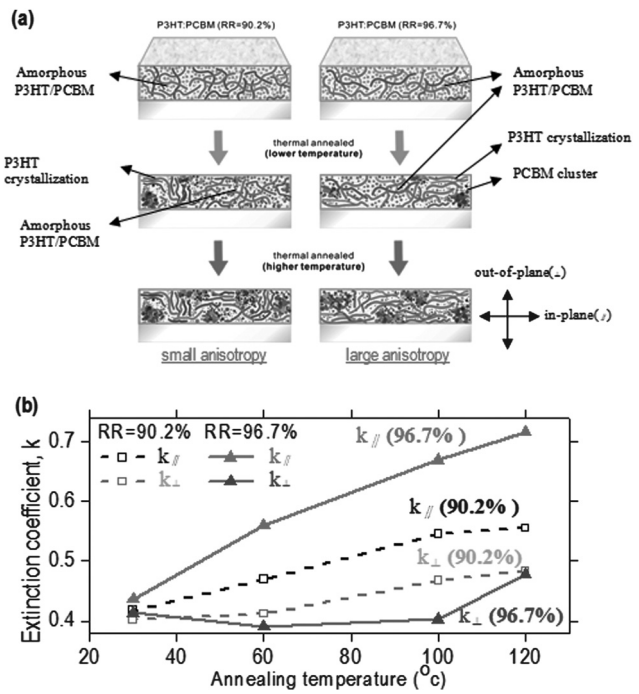

Fig. 8 (a) Schematic representation of the morphological transformation of the 90.2% and 96.7% RR P3HT/PCBM hybrid films. (b) In-plane and out-of-plane extinction coefficients of the 90.2% and 96.7% RR P3HT/PCBM hybrid films plotted with respect to the annealing temperature.

that the amorphous morphology converted to polymer crystallinity in both the in-plane and out-of-plane orientations. Because the preferential orientation lies parallel to the substrate, we observed a larger enhancement in the value of $k_{\parallel}$ relative to that

Table 1 Properties of high- and low-RR P3HT/PCBM-based photovoltaic devices prepared with variously sized active areas

Area (mm^2)	RR (%)	V_{oc} (V)	J_{sc} (mA/cm^2)	FF (%)	η (%)
4	90.2%	0.60	7.93	57.77	2.75
4	96.7%	0.64	11.15	57.16	3.86
50	90.2%	0.56	6.58	39.00	1.44
50	96.7%	0.60	6.50	41.69	1.78
100	90.2%	0.62	4.22	29.31	0.77
100	96.7%	0.59	5.65	31.62	1.06
200	90.2%	0.61	3.07	26.78	0.50
200	96.7%	0.58	5.60	31.65	1.02
400	96.7%	0.59	5.73	28.17	0.96

of $k_{\perp}$. Moreover, the RR effect is clear: the significant difference between the enhancements in the values of $k_{\parallel}$ and $k_{\perp}$ for the 96.7% RR P3HT/PCBM blend reveals that the better close packing ability results in a pronounced in-plane extension and alignment during the crystallization process. Fig. 8 (a) displays the hybrid structures of the high- and low-RR samples during their morphological conversion under thermal annealing. The high-RR P3HT polymer crystallized mainly parallel to the substrate; the low-RR polymer formed both parallel and perpendicular crystallinity domains. Thus, anisotropic optical absorption phenomena revealed two distinct morphological transformations that resulted in changes to the anisotropic properties of the high- and low-RR polymers, respectively. The morphological transformations of the low- and high-RR P3HT/PCBM blends had a profound influence on the performance of organic BHJ photovoltaic devices. Table 1 lists the relationship between the conversion efficiency and the RR for devices featuring various active areas (from 4 to 400 mm^2). Solar cells possessing layered structures of BK7/ITO (140 nm)/PEDOT (30 nm)/P3HT:PCBM (85 nm)/Al (100 nm) were fabricated in air. We measured the current density–voltage (J–V) characteristics of the 90.2% and 96.7% RR P3HT/PCBM blend devices under simulated AM1.5 illumination conditions. Table 1 summarizes the values of the short-circuit current density (J_{sc}), the open-circuit voltage (V_{oc}), the filling factor (FF), and the PCE (η) obtained from these measurements. The highest values of J_{sc} (11.15 mA/cm^2) and η (3.86) were achieved for the 96.7% RR P3HT/PCBM blend device having an active area of 4 mm^2. Indeed, all of the samples, regardless of the size of their active areas, revealed that the presence of the higher-RR P3HT polymer has a positive effect on the PCE. Moreover, the influence of the RR was more obvious in the samples having larger active areas. We attribute this behavior to the significant enhancement of the anisotropic properties of the high-RR P3HT polymer after thermal annealing. The preferential in-plane (‖) orientation of the P3HT main chains results in stronger optical absorption *via* π–π* resonance for incident light aligned normal to the substrate. Indeed, the tendency toward crystalline closer packing during thermal annealing appears to enhance the optical absorption and carrier mobility of the P3HT/PCBM blend, leading to higher PCE.

Conclusions

We have characterized the optical anisotropy of high- and low-RR P3HT/PCBM hybrid films before and after their thermal annealing as a potentially useful and convenient strategy to determine the anisotropic morphologies present in hybrid organic solar cells. Ellipsometry and polarized optical spectral measurements revealed that the high-RR P3HT/PCBM blend exhibited a highly anisotropic extinction coefficient, *i.e.*, a high ratio between the in-plane and out-of-plane intensities of the peak representing the π–π* optical absorption. After annealing to 120 °C, the degrees of anisotropy of the 90.2% and 96.7% RR P3HT/PCBM blends were represented by values of $k_{\parallel}/k_{\perp}$ of 1.09 and 1.59, respectively; *i.e.*, a pronounced anisotropy for the high-RR system. Moreover, the degrees of anisotropy clearly revealed that different morphological conversion processes occurred for the high- and low-RR P3HT/PCBM blends during thermal annealing, with the high-RR P3HT polymer's morphology converting from amorphous to preferentially extended and aligned parallel to the substrate in the PCBM-free regions. In contrast, the low-RR P3HT/PCBM blend provided P3HT polymer crystallites aligned both parallel and perpendicular to the substrate. Thus, the RR affects the extent of polymer main chain orientation during thermal annealing. Additionally, the presence of the higher-RR P3HT had significant positive effects on the current density and voltage characteristics of P3HT/PCBM-based solar cells. The relationship between the conversion efficiency and the RR was more pronounced in solar cells featuring large active areas. On the basis of these results, the use of high-RR P3HT enhances the anisotropic optical absorption and PCE of solar cells.

Acknowledgements

We thank the National Science Council, Taiwan, R.O.C., for supporting this study under contracts NSC-97-2221-E-002-046-MY3 and 98-2623-E-002 -001-ET.

References

1 J. U. Lee, A. Cirpan, T. Emrick, T. P. Russell and W. H. Jo, *J. Mater. Chem.*, 2009, **19**, 1483.
2 G. Yu, J. Gao, J. C. Hummelen, F. Wudl and A. J. Heeger, *Science*, 1995, **270**, 1789.
3 W. L. Ma, C. Y. Yang, X. Gong, K. Lee and A. J. Heeger, *Adv. Funct. Mater.*, 2005, **15**, 1617.
4 G. Dennler, M. C. Scharber and C. J. Brabec, *Adv. Mater.*, 2009, **21**, 1323.
5 L. M. Chen, Z. Hong, G. Li and Y. Yang, *Adv. Mater.*, 2009, **21**, 1.
6 M. Campoy-Quiles, T. Ferenczi, T. Agostinelli, P. G. Etchegoin, Y. Kim, T. D. Anthopoulos, P. N. Stavrinou, D. D. C. Bradley and J. Nelson, *Nature Mater.*, 2008, **7**, 158.
7 C. N. Hoth, P. Schilinsky, S. A. Choulis and C. J. Brabec, *Nano Lett.*, 2008, **8**, 2806.
8 Y. Kim, S. A. Choulis, J. Nelson, D. D. C. Bradley, S. Cook and J. R. Durrant, *Appl. Phys. Lett.*, 2005, **86**, 063502.
9 A. J. Moule and K. Meerholz, *Adv.Mater.*, 2008, **20**, 240.
10 L. Li, G. Lu and X. Yang, *J. Mater. Chem.*, 2008, **18**, 1984.
11 V. Shrotriya, G. Li, Y. Yao, T. Moriarty, K. Emery and Y. Yang, *Adv. Funct. Mater.*, 2006, **16**, 2016.
12 Y. M. Chang, W. F. Su and L. Wang, *Sol. Energy Mater. Sol. Cells*, 2008, **92**, 761.
13 C. W. Chu, H. Yang, W. J. Hou, J. Huang, G. Li and Y. Yang, *Appl. Phys. Lett.*, 2008, **92**, 103306.
14 P. J. Brown, D. S. Thomas, A. Kohler, J. S. Wilson, J. S. Kim, C. M. Ramsdale, H. Sirringhaus and R. H. Friend, *Phys. Rev. B*, 2003, **67**, 064203.
15 U. Zhokhavets, G. Gobsch, H. Hoppe and N. S. Sariciftci, *Synth. Met.*, 2004, **143**, 113.

16 R. C. Hiorns, R. de Bettignies, J. Leroy, S. Bailly, M. Firon, C. Sentein, A. Khoukh, H. Preeud'homme and C. Dagron-Lartigau, *Adv. Funct. Mater.*, 2006, **16**, 2263.
17 C. J. Ko, Y. K. Li and F. C. Chen, *Adv. Mater.*, 2007, **19**, 3520.
18 Y. Kim, A. M. Ballantyne, J. Nelson and D. D. C. Bradley, *Org. Electron.*, 2009, **10**, 205.
19 G. Li, Y. Yao, H. Yang, V. Shrotriya, G. Yang and Y. Yang, *Adv. Funct. Mater.*, 2007, **17**, 1636.
20 G. Li, V. Shrotriya, J. Huang, Y. Yao, T. Moriarty, K. Emery and Y. Yang, *Nature. Mater.*, 2005, **4**, 864.
21 S. Miller, G. Fanchini, Y. Y. Lin, C. Li, C. W. Chen, W. F. Su and M. Chhowalla, *J. Mater.Chem.*, 2008, **18**, 306.
22 T. Erb, U. Zhokhavets, G. Gobsch, S. Raleva, B. Stuhn, P. Schilinsky, C. Waldauf and C. J. Brabec, *Adv. Funct. Mater.*, 2005, **15**, 1193.
23 G. Li, V. Shrotriya, Y. Yao, J. Huang and Y. Yang, *J. Mater. Chem.*, 2007, **17**, 3126.
24 Y. Kim, S. Cook, S. M. Tuladhar, S. A. Choulis, J. Nelson, J. R. Durrant, D. D. C. Bradley, M. Giles, I. Mcculloch, C. S. Ha and M. Ree, *Nature Mater.*, 2006, **5**, 197.
25 A. M. Ballantyne, L. Chen, J. Dane, T. Hammant, F. M. Braun, M. Heeney, W. Duffy, I. McCulloch, D. D. C. Bradley and J. Nelson, *Adv. Funct. Mater.*, 2008, **18**, 2373.
26 D. Comoretto, R. Tubino, G. Dellepiane, G. F. Musso, A. Borghesi, A. Piaggi and G. Lanzani, *Phys. Rev. B*, 1990, **41**, 3534.
27 M. Tarmmer and A. P. Monkman, *Adv.Mater.*, 2002, **14**, 210.
28 C. M. Ramsdale and N. C. Greenham, *Adv. Mater.*, 2002, **14**, 212.
29 J. M. Winfield, C. L. Donley and J. S. Kim, *J. Appl. Phys.*, 2007, **102**, 063505.
30 U. Zhokhavets, G. Gobsch, H. Hoppe and N. S. Sariciftci, *Synth. Met.*, 2004, **143**, 113.
31 C. Soci, D. Comoretto, F. Marabelli and D. Moses, *Phys. Rev. B*, 2007, **75**, 075204.
32 U. Zhokhavets, T. Erb, H. Hoppe, G. Gobsch and N. S. Sariciftci, *Thin Solid Films*, 2006, **496**, 679.
33 M. Urien, L. Bailly, L. Vignau, E. Cloutet and A. de Cuendias, *Polym. Int.*, 2008, **57**, 764.
34 C. H. Woo, B. C. Thompson, B. J. Kim, M. F. Toney and J. M. J. Frechet, *J. Am. Chem. Soc.*, 2008, **130**, 16324.

